Evidence for unusually thin oceanic crust and strong mantle beneath the Amazon Fan

M. Rodger
A.B. Watts
Department of Earth Sciences, University of Oxford, Parks Road, Oxford OX1 3PR, UK
C.J. Greenroyd
C. Peirce
R.W. Hobbs
Department of Earth Sciences, University of Durham, South Road, Durham DH1 3LE, UK

ABSTRACT

We used seismic and gravity data to determine the structure of the crust and mantle beneath the Amazon Fan. Seismic data suggest that the crust is of oceanic-type and is unusually thin (<~4 km) compared to elsewhere in the Atlantic. We attribute the thin crust to ultraslow seafloor spreading following the breakup of South America and Africa during the Early Cretaceous. Gravity data suggest that the fan was emplaced on lithosphere that increased its elastic thickness, T_e, and hence strength, following rifting. The increase, from 10 km to 40 km, is greater, however, than would be expected if T_e were determined by a single controlling isotherm, based on a cooling plate model. Hence, we conclude that the Amazon Fan has been emplaced on, and is supported by, unusually thin oceanic crust and strong mantle.

Keywords: Amazon Fan, crustal structure, mantle, gravity anomalies, isostasy.

INTRODUCTION

The manner in which Earth's outermost layers support large river deltas has been a topic of debate ever since the pioneering work of Joseph Barrell on the Devonian of the Catskill Mountains. Barrell (1914) argued that modern deltas such as the Nile and Niger were fully supported by the strength of the crust and mantle. Bowie (1922), however, suggested that the crust and mantle would yield locally under their weight. Although the small-amplitude free-air gravity anomalies that are observed over deltas favor the Bowie model, the lack of seismic data on their deep structure has limited our understanding of exactly how such large loads are supported.

The Amazon Delta and its associated deep-sea fan constitute one of the world's largest sedimentary systems. The fan comprises sediment derived from the Amazon River that drains much of the northern half of South America. Previous studies have shown that the fan has grown by the superposition of a number of broad levee complexes (Damuth et al., 1983) and is underlain by >8 km of late Miocene and younger sediment (Houtz et al., 1977).

During November–December 2003, onboard RRS *Discovery*, we acquired the first coincident multichannel seismic-reflection and refraction data over the fan (Fig. 1). Cruise D275 was equipped with a 102 L, 14 element, air-gun array, a 2.4-km-long streamer, and 39 IFM-GEOMAR ocean-bottom seismometers and hydrophones (OBSs and OBHs). Here we use the seismic data to determine the structure of the crust and mantle beneath the fan.

DATA

Figure DR1 (see GSA Data Repository[1]) shows seismic-reflection profile line B, which was acquired across the middle and lower part of the fan. Oceanic basement is recognized as a series of high-amplitude irregular and rough reflectors that generally dip landward, in a SW direction. Overlying oceanic basement is a wedge, ~1.5–5.0 s two-way traveltime (TWTT) thick, of well-stratified sediments, which thin seaward, in a NE direction. Within the lower part of the wedge, reflector terminations define a major angular unconformity (U_d).

Unconformity U_d has been recognized in previous reflection data (Damuth, 1975; Castro et al., 1978; Braga, 1991), and it has been attributed to the superposition on the margin of clastic sediments derived from the Amazon river at ca. 10 Ma (Cobbold et al., 2004). The most probable source of the sediment was uplift and erosion in the Bolivian Andes (Benjamin et al., 1987) that blocked drainage of the Amazon basin into the Pacific and redirected it into the Atlantic.

Other commercial seismic data show that the margin developed following breakup and the rifting apart of South America and Africa during the Early Cretaceous (Pereira da Siva, 1989; Mello et al., 2001; Cobbold et al., 2004). Evidence for rifting is recorded on the inner shelf, where a synrift, mainly coarse clastic sequence of ca. 100–115 Ma age is overlain by a postrift, mainly fan-delta and platform car-

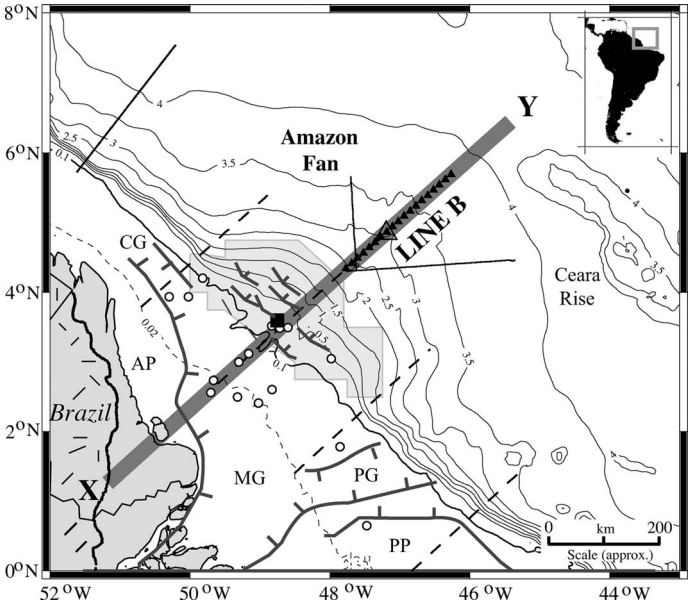

Figure 1. Location map of Amazon Fan. Contours show bathymetry at 0.5 km intervals, except on shelf, where only 0.02 and 0.10 m contours are shown. Thick gray line shows location of profile X-Y modeled in Figure 4. Filled black triangles show ocean-bottom seismometers and hydrophones (OBSs and OBHs) along line B. Large triangle shows OBS 315, arrivals at which are shown in Figure 2. Solid lines show location of other reflection lines acquired during D275. Dashed lines show location of Petrobrás 18 s reflection lines. Light-gray shaded region shows BP survey area. Tectonic elements (gray lines) are based on Carozzi (1981). Gray lines with short bars show Miocene growth faults near shelf break. Gray lines with long bars show location of Caciporé (CG), Mexiana (MG), and Pará (PG) synrift grabens. AP—Amapá platform, PP—Pará platform. Open circles show selected Petrobrás wells. Filled square shows the location of "point A" of Silva and Maciel (1998). The hachured region onshore shows Early/Middle Proterozoic basement rock outcrop.

[1]GSA Data Repository item 2006234, seismic reflection profile data, structure, and gravity anomaly maps is available online at www.geosociety.org/pubs/ft2006.htm, or on request from editing@geosociety.org or Documents Secretary, GSA, P.O. Box 9140, Boulder, CO 80301–9140, USA.

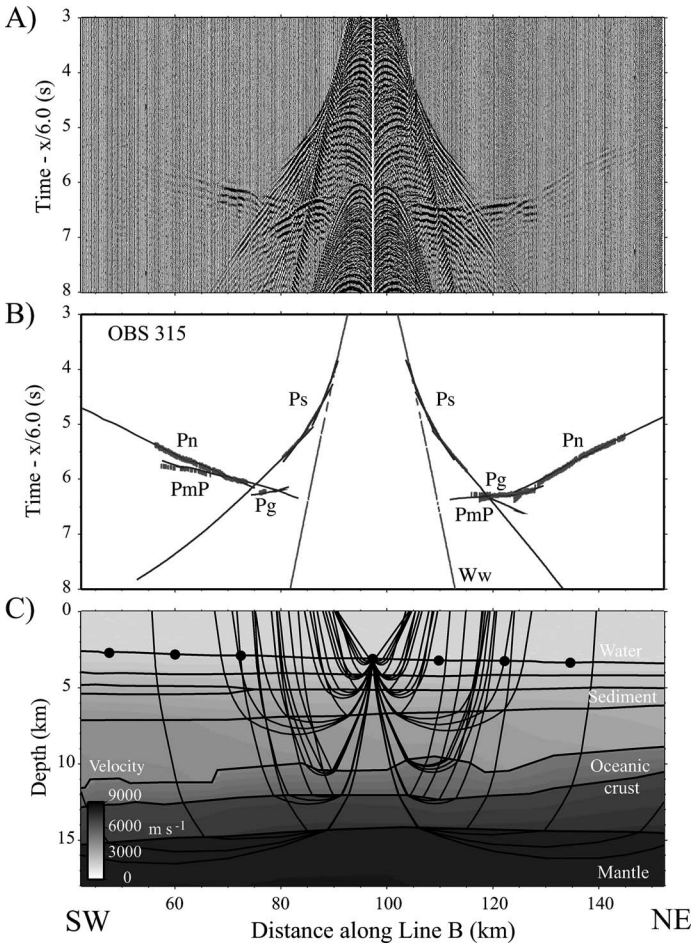

Figure 2. Seismic data recorded on hydrophone component of OBS 315 in middle part of the fan (Figs. 1 and DR1 [see text footnote 1]). A: Band-pass filtered data. Data are plotted with a reduction velocity of 6.0 km s^{-1}. B: Picked (thick lines with pick error bars) and modeled arrivals (thin lines), showing Ww, Ps, Pg, Pn, and PmP arrivals. Modeled arrivals have been computed using velocity model shown in Figure 3. Note limited range (~5 km) over which Pg event appears as a first arrival, due to a combination of relatively high velocities in lower part of sediment wedge and unusually thin oceanic crust that underlies it. C: Ray diagram of the best-fit velocity model.

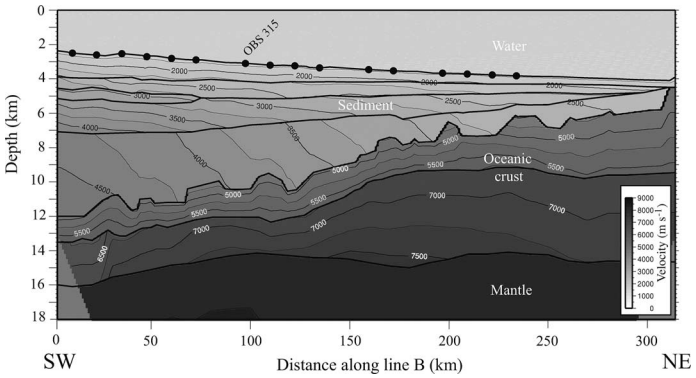

Figure 3. Best-fit velocity model for all 16 ocean-bottom seismometers and hydrophones (OBSs and OBHs) along line B (Fig. DR1, see text footnote 1). RMS traveltime difference between observed and calculated arrivals was 0.027 s, and normalized chi-squared was 1.135. Other statistical parameters are summarized in Table DR1 (see text footnote 1). Thick lines show model layer boundaries that are generally marked by small increments in velocity. Thin lines show velocity contours at 0.25 km s^{-1} intervals.

bonate sequence of 0–100 Ma age (Brandão and Feijó, 1994). The Amazon Fan was therefore emplaced on a passive margin ca. 90–105 Ma, after rifting.

SEISMIC MODELING

We have used the reflection data, together with the refracted arrivals at 16 OBSs and OBHs deployed along line B to determine the sediment, crustal, and upper-mantle structure beneath the middle and lower parts of the fan.

Figure 2 shows seismic-refraction profile data for OBS 315 along line B. The OBS shows the water wave (Ww) and the sediment (Ps), crust (Pg), and mantle (Pn) arrivals out to ranges of ~50 km, as well as Moho reflections (PmP). The velocity structure that best fits the observed arrivals was determined using a forward modeling method combined with RAYINVR of Zelt and Smith (1992).

Figure 3 shows the resulting, preferred P-wave velocity model. Underlying the fan are sediment and crustal layers. The sediments can be subdivided on the basis of their bounding velocity gradients into four layers with velocities that range from 1.7 to 4.5 km s^{-1}. Unconformity U_d (Fig. DR1, see footnote 1) occurs approximately at the interface between the third and fourth layers. There is evidence that velocities decrease in a seaward direction, especially in the layers above the unconformity. We attribute these variations, at least in part, to facies changes.

The upper crust correlates with velocities in the range 4.5–5.7 km s^{-1}. Unlike the overlying sediments, the upper crust shows little lateral variation in velocity. The transition to the lower crust is marked by an abrupt change from a high-gradient (~0.75 s^{-1}) to a low-gradient (~0.15–0.25 s^{-1}) layer, which is accompanied by a step in velocity to >6.7 km s^{-1}. Velocities then increase to ~7.3 km s^{-1} at the base of the crust. The lower crust shows much smaller variations in velocities than the upper crust. Again, there is little evidence of lateral changes in velocity. The upper- and lower-crustal velocities are typical of Atlantic oceanic crust (e.g., White et al., 1992), and so we interpret the crust that underlies the thick sedimentary layers along line B as oceanic in type.

The transition from oceanic crust to mantle is marked by a step in velocity to >8.0 km s^{-1}. Crustal thickness changes abruptly along line B (Fig. 3). Landward of ~140 km, the crust is relatively thin (4.2 ± 0.4 km), while seaward, it is relatively thick (7.6 ± 1.0 km), close to the normal thickness of Atlantic oceanic crust. Line B is located just to the west of the Ceara Rise, which is an aseismic ridge (conjugate to the Sierra Leone Rise) that formed on or near the Mid-Atlantic Ridge ca. 80 Ma (Campanian) (Kumar and Embley, 1977). The thick crust may therefore reflect this excess volcanism.

The origin of the thin oceanic crust is not as clear. Elsewhere in the Atlantic, such crust is restricted to fracture zones (Detrick and Purdy, 1980) and certain nonvolcanic margins (Whitmarsh et al., 1996; Hopper et al., 2006).

The NE Brazil margin developed in close proximity to the Equatorial Atlantic fracture zone (Sibuet and Mascle, 1978), and there is evidence in the satellite-derived gravity field (Sandwell and Smith, 1997) that the Doldrum's and St. Paul fracture zones intersect the margin to the north and south of the fan. There is no evidence, however, of any fracture zone intersecting line B. Moreover, we do not see either the low velocities in the upper part of layer 2 or the absence of a layer 3 refractor, as reported by Detrick and Purdy (1980) at the Kane fracture zone. Finally, we have imaged thin oceanic crust on other margin profiles (Greenroyd et al., 2005), suggesting an areal extent much greater than found at fracture zones.

The seismic structure most closely resembles the thin oceanic crust that abuts the Peridotite Ridge at the Galicia Bank and thin continental crust at the Flemish Cap margins. We therefore follow Hopper et al. (2004) and suggest that the thin oceanic crust reflects a limited

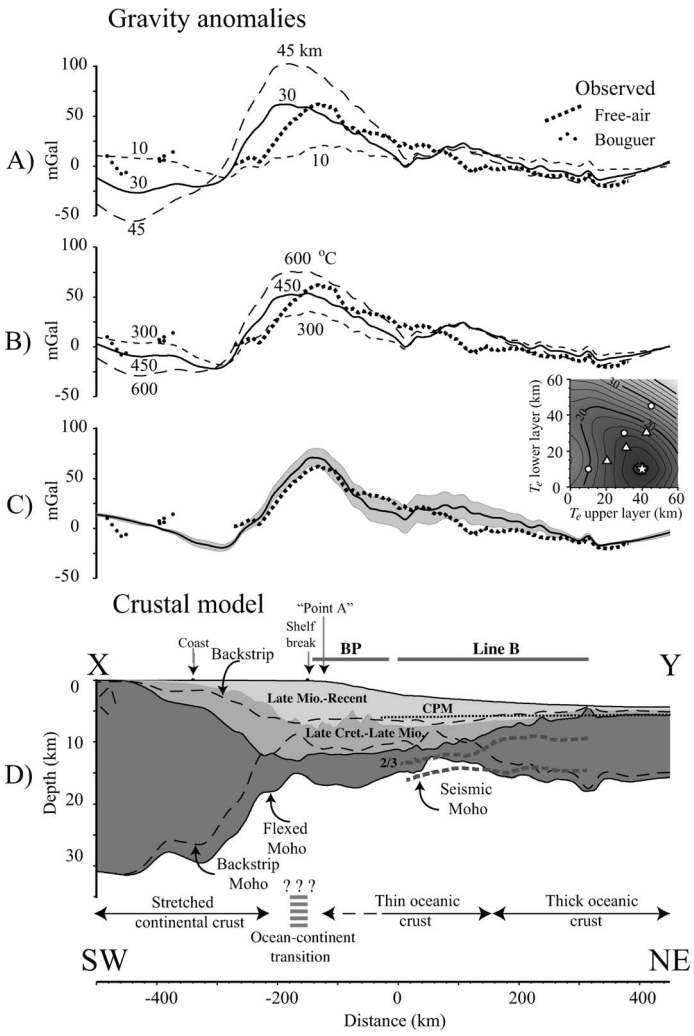

Figure 4. Comparison of observed and calculated gravity anomalies along profile X-Y (Fig. 1). Observed gravity is based on shipboard (thick dashed line) and GETECH land data (filled circles) and has had a long wavelength field, complete to degree and order 20, subtracted from it. Calculated gravity (solid and thin dashed lines and shaded region) is based on parameters listed in Table 1 and either a constant T_e or one that varies with age. A: Constant T_e. T_e = 10 km (short dashed line), T_e = 30 km (solid line), T_e = 45 km (long dashed line). B: Cooling plate model. $T_e = Z_{300\,°C}$ (short dashed line), $T_e = Z_{450\,°C}$ (solid line), $T_e = Z_{600\,°C}$ (long dashed line). C: T_e varies with age since rifting. T_e (Late Cretaceous–late Miocene, lower layer) = 10 km, T_e (late Miocene–Holocene, upper layer) = 40 km. Shaded region shows effect of varying sediment density by ±100 kg m^{-3}. D: Crustal model corresponding to best-fit model in C. CPM—expected depth of oceanic crust based on cooling plate model. 2/3—step in velocity that defines transition from upper to lower oceanic crust. Inset shows RMS difference between observed and calculated gravity anomalies. White filled circles—constant T_e model. White filled triangles—cooling plate model. White filled star—best-fit model with T_e = 10 km for lower layer and T_e = 40 km for upper layer.

magma supply at an ultraslow-spreading ridge, similar in setting to that occurring at the present-day southwest Indian and Gakkel Ridges (Dick et al., 2003).

What distinguishes NE Brazil from these other margins is its association with thick sediments. We do not believe, however, that crustal thinning due to extension has caused excess subsidence, although such a process may have enhanced it. Rather, we believe that the crust was already thin prior to sediment loading. If this is so, despite its unusual thickness, the oceanic crust together with its underlying mantle must be strong enough to support the load of the fan.

TABLE 1. SUMMARY OF PARAMETERS USED IN THE FLEXURE

Density of seawater = 1030 kg
Density of upper sediment layer = 2170
Density of lower sediment layer = 2450
Average age of younger, upper sediment
Average age of older, lower sediment layer
Average age of oceanic lithosphere loaded by sediments
Density of crust = 2800 kg m
Thickness of zero elevation continental crust
Density of mantle = 3330 kg
Young's Modulus = 100 GPa
Poisson's ratio = 0.25

FLEXURAL BACKSTRIPPING AND GRAVITY MODELING

We used the seismic data, together with 3-dimensional (3-D) backstripping and gravity modeling techniques (Stewart et al., 2000), to determine the effective elastic thickness, T_e, and, hence, the strength of the crust and mantle beneath the fan. First, depth-converted reflector picks from line B were combined with the BP data (P. Bentham, June 2004, personal commun.; Fig. 1) and used to construct structure maps (Fig. DR2, see footnote 1) and then isopachs for an older Late Cretaceous–late Miocene layer and a younger late Miocene–Recent layer. Next, each layer was backstripped for different values of T_e, and the cumulative tectonic subsidence and uplift was used to isostatically restore the crustal structure at the time of rifting, assuming an Airy model. The final step was to constrain T_e by calculating the combined gravity effect of rifting and sediment loading and its compensation and comparing it to the observed gravity anomaly.

Figure 4 compares observed and calculated gravity anomalies along profile X-Y (Fig. 1). The calculated anomaly is based on a T_e that is either constant for each layer (Fig. 4A) or varies with age (Figs. 4B and 4C). We found a constant T_e model with T_e = 30 km explains the observations well (root mean square [RMS] difference between observed and calculated gravity = 14.5 mGal). This T_e is similar to that estimated by Cochran (1973), but is smaller than the 38.0 km assumed by Driscoll and Karner (1994). There are discrepancies, however. The calculated gravity is too high (by ~40 mGal) on the landward side of the observed high and too low (by ~25 mGal) on the seaward side (Fig. 4A). Furthermore, the peak in the observed high appears to be displaced by ~50 km seaward of the calculated high. Interestingly, the younger, upper sediment layer depocenter is also shifted seaward of the older, lower layer.

In order to explain the discrepancies, we constructed models in which each layer had a different, rather than the same, T_e. Figure 4B compares the observed and calculated gravity for a model in which T_e is given by depth to the 450 °C isotherm (i.e., $T_e = Z_{450\,°C}$), based on a cooling plate model (Table 1). This model reduces the RMS difference to 12.2, compared with 14.5 mGal. However, the calculated high is still displaced, albeit by a smaller amount (25 compared to 50 km). Figure 4C shows a model in which the T_e of the lower and upper layer is smaller (10 km) and greater (40 km), respectively. This model has a smaller RMS difference (9.4 mGal) and, importantly, brings the peak of both the observed and calculated high on profile X-Y into better agreement.

The calculated profile in Figure 4C assumes a uniform density for the sediment and crustal layers. The velocity model (Fig. 3) suggests this to be a reasonable assumption for the crustal, but not the sediment layer. We therefore show (shaded region) the calculated gravity effect of the best fit T_e model for a range of densities from 2350 to 2550 kg m^{-3} for the lower layer and 2070–2270 kg m^{-3} for the upper layer. The figure suggests that lateral density changes may be large enough to explain some of the discrepancies that remain in the best-fit T_e model (e.g., at −20 km and 100 km).

DISCUSSION

Our best-fit T_e model has implications for the subsidence and uplift history, the crust and mantle structure, and the long-term mechanical properties of the NE Brazil margin.

Müeller et al.'s (1997) age grid suggests that the oceanic crust increases in age from ca. 85 Ma at the seaward end of line B to ca. 105 Ma at −40 km along line B. We therefore used the cooling plate model to compute the subsidence expected for 85–105 Ma oceanic crust and compared it to the total tectonic subsidence derived from flexural backstripping. Figure 4D shows that the two subsidence calculations agree well. The main departures are at 60 km, where the crust is relatively thin, and 300 km, where the crust is relatively thick, and so can be explained by crustal thickness variations.

The backstripping of stratigraphic data at "point A" (Fig. 1) reveals an oceanic-type subsidence curve, suggesting that oceanic crust may extend landward of −40 km, to the shelf break at −125 km (Fig. 4D). In addition, our best-fit model suggests that thin crust extends landward as far as ~–200 km beneath the outer shelf, where it abuts thick, presumably continental, crust.

Unfortunately, it is not possible using the existing seismic data to precisely locate the ocean-continent transition between −125 and −200 km. The seismic-line drawings of Pereira da Siva (1989) showed rotated blocks bounded by normal faults beneath the shelf break region, but the BP seismic-reflection profile data (e.g., profile 2 of Cobbold et al., 2004) do not show clear evidence of their associated synrift sequences.

The flexure caused by the Amazon Fan load reaches ~6 km and involves both oceanic and continental crust. Rock mechanics data (e.g., Goetze and Evans, 1979) suggest that while thin oceanic crust might be strong, it would be unable to support the high curvatures (7×10^{-7} m^{-1}) implied by such a flexure and that the subcrustal mantle lithosphere must be involved. The T_e increase required to explain the gravity anomalies, however, is greater than would be expected for suboceanic mantle, and might reflect incomplete isostatic relaxation of the relatively thick sequence of Pleistocene and younger sediments that comprise the fan load. Alternatively, the increase could reflect the influence of the rheological properties of the subcontinental mantle. Indeed, our T_e estimates are compatible with the model predictions of Burov and Poliakov (2001), who suggested that extension-induced heating of continental lithosphere causes a T_e decrease during the synrift phase and replacement of weak crust by mantle causes a T_e increase during the postrift phase.

ACKNOWLEDGMENTS

We thank the master, officers, and crew of RRS *Discovery*, the UK Ocean Research Services technicians, and T. Oliva (SEAMAP, UK), A. Krabbenhoeft, and C. Papenberg (IFM-GEOMAR) for their help at sea, P. Bentham and D. Fairhead for access to BP and GETECH data, and J. Hopper and P. Cobbold for their constructive reviews. This work was supported by the Natural Environment Research Council NERC/LINK Ocean Margins program.

REFERENCES CITED

Barrell, J., 1914, The strength of the Earth's crust. V. The depth of masses producing gravity anomalies and deflection residual: The Journal of Geology, v. 22, p. 441–468, 537–555.

Benjamin, M.T., Johnson, N.M., and Naeser, C.W., 1987, Rapid uplift in the Bolivian Andes: Geology, v. 15, p. 680–683.

Bowie, W., 1922, The Earth's crust and isostasy: Geographical Review, v. 12, p. 613–627.

Braga, L.F.S., 1991, Isostatic evolution and crustal structure of the Amazon continental margin determined by admittance analyses and inversion of gravity data [Ph.D. thesis]: Corvallis, Oregon, Oregon State University, 161 p.

Brandão, J.A.S.L., and Feijó, F.J., 1994, Bacia da Foz do Amazonas: Boletim de Geosciências da Petrobrás, v. 8, p. 91–99.

Burov, E., and Poliakov, A., 2001, Erosion and rheology controls on synrift and postrift evolution: Verifying old and new ideas using a fully coupled numerical model: Journal of Geophysical Research, v. 106, p. 16,461–16,481, doi: 10.1029/2001JB000433.

Carozzi, A.V., 1981, Porosity models and oil exploration of Amapa carbonates, Paleogene, Foz do Amazonas basin, offshore NW Brazil: Journal of Petroleum Geology, v. 4, p. 3–34.

Castro, J.C., Miura, K., and Braga, J.A.E., 1978, Stratigraphic and structural framework of the Foz do Amazonas basin, *in* Society of Petroleum Engineers 10th Annual Offshore Technology Conference Proceedings, Houston, Texas, v. 3, p. 1843–1847.

Cobbold, P.R., Mourgues, R., and Boyd, K., 2004, Mechanism of thin-skinned detachment in the Amazon Fan: Assessing the importance of fluid overpressure and hydrocarbon generation: Marine and Petroleum Geology, v. 21, p. 1013–1025.

Cochran, J.R., 1973, Gravity and magnetic investigations in the Guiana Basin, Western Equatorial Atlantic: Geological Society of America Bulletin, v. 84, p. 3249–3268.

Damuth, J.E., 1975, Amazon Cone: Morphology, sediments, age and growth pattern: Geological Society of America Bulletin, v. 86, p. 863–878.

Damuth, J.E., Kowsmann, R.O., Flood, R.D., Belderson, R.H., and Gorini, M.A., 1983, Age relationships of distributary channels on Amazon deep-sea fan: Implications for fan growth pattern: Geology, v. 11, p. 470–473.

Detrick, R.S., and Purdy, G.M., 1980, The structure of the Kane fracture zone from seismic refraction studies: Journal of Geophysical Research, v. 85, p. 3759–3778.

Dick, H.J.B., Lin, J., and Schouten, H., 2003, An ultraslow-spreading class of ocean ridge: Nature, v. 426, p. 405–412, doi: 10.1038/nature02128.

Driscoll, N.W., and Karner, G.D., 1994, Flexural deformation due to Amazon Fan loading: A feedback mechanism affecting sediment delivery to margins: Geology, v. 22, p. 1015–1018.

Goetze, C., and Evans, B., 1979, Stress and temperature in the bending lithosphere as constrained by experimental rock mechanics: Geophysical Journal of the Royal Astronomical Society, v. 59, p. 463–478.

Greenroyd, C.J., Peirce, C., Rodger, M., Watts, A.B., and Hobbs, R.W., 2005, Crustal structure of the continental margin offshore French Guiana, central Atlantic [abs.]: Eos (Transactions, American Geophysical Union), v. 86., doi: 2005AGUFM.T43B1403G.

Hopper, J.R., Funck, T., Tucholke, B.E., Larsen, H.C., Holbrook, W.S., Louden, K.E., Shillington, D., and Lau, H., 2004, Continental break-up and the onset of ultraslow seafloor spreading off Flemish Cap on the Newfoundland rifted margin: Geology, v. 32, p. 93–96, doi: 10.1130/G19694.1.

Hopper, J.R., Funck, T., Tucholke, B.E., Louden, K.E., Holbrook, W.S., and Larsen, H.C., 2006, A deep seismic investigation of the Flemish Cap margin: Implications for the origin of deep reflectivity and evidence for asymmetric breakup between Newfoundland and Iberia: Geophysical Journal International, v. 164, p. 501–515, doi: 10.1111/j.1365-246X.2006.02800.x.

Houtz, R.E., Ludwig, W.J., Milliman, J.D., and Grow, J.A., 1977, Structure of the northern Brazilian continental margin: Geological Society of America Bulletin, v. 88, p. 711–719.

Kumar, N., and Embley, R.W., 1977, Evolution and origin of Ceara Rise: An aseismic rise in the western equatorial Atlantic: Geological Society of America Bulletin, v. 88, p. 683–694.

Mello, M.R., Silva, S.R.P., Miranda, F.P., Mossmann, R., and Maciel, R.R., 2001, Foz do Amazonas area: The last frontier for elephant hydrocarbon accumulations in the South Atlantic realm, *in* Downney, J.C., Threet, J.C., and Morgan, W.A., eds., Petroleum Provinces of the 21st Century: American Association of Petroleum Geologists Memoir 74, p. 403–414.

Müeller, R.D., Roest, W.R., Royer, J.-Y., Gahagan, L.M., and Sclater, J.G., 1997, Digital isochrons of the world's ocean floor: Journal of Geophysical Research, v. 102, p. 3211–3214, doi: 10.1029/96JB01781.

Pereira da Siva, S.R., 1989, Bacias da Foz do Amazonas e Para (Aguas Profundas): Una anlise sismoestratigrafica, tectonsedimentar e termica: Conference Proceedings of the Brazilian Geological Society, v. 2, p. 843–852.

Sandwell, D.T., and Smith, W.H.F., 1997, Marine gravity anomaly from Geosat and ERS-1 satellite altimetry: Journal of Geophysical Research, v. 102, p. 10,039–10,054, doi: 10.1029/96JB03223.

Sibuet, J.-C., and Mascle, J., 1978, Plate kinematic implications of Atlantic equatorial fracture zone trends: Journal of Geophysical Research, v. 83, p. 3401–3421.

Silva, S.R.P., and Maciel, R.R., 1998, Foz do Amazonas basin hydrocarbon system: American Association of Petroleum Geologists International Conference & Exhibition, Rio de Janeiro, Brazil, Extended abstracts, p. 480–481.

Stewart, J., Watts, A.B., and Bagguley, J., 2000, Three-dimensional subsidence analysis and gravity modelling of the continental margin offshore Namibia: Geophysical Journal International, v. 141, p. 724–746, doi: 10.1046/j.1365-246x.2000.00124.x.

White, R.S., McKenzie, D., and O'Nions, R.K., 1992, Oceanic crustal thickness from seismic measurements and rare earth element inversions: Journal of Geophysical Research, v. 97, p. 19,683–19,715.

Whitmarsh, R.B., White, R.S., Horsefield, S.J., Sibuet, J.-C., Recq, M., and Louvel, V., 1996, The ocean-continent boundary off the western continental margin of Iberia: Crustal structure west of Galicia: Journal of Geophysical Research, v. 101, p. 28,291–28,314, doi: 10.1029/96JB02579.

Zelt, C.A., and Smith, R.B., 1992, Seismic traveltime inversion for 2-D crustal velocity structure: Geophysical Journal International, v. 108, p. 16–34.

Manuscript received 14 May 2006
Revised manuscript received 1 August 2006
Manuscript accepted 2 August 2006

Printed in USA